

Supporting Information

Growth of 2D Mesoporous Polyaniline with Controlled Pore Structures on Ultrathin MoS₂ Nanosheets by Block Copolymer Self-Assembly in Solution

Hao Tian^a, Shuyan Zhu^a, Fugui Xu^a, Wenting Mao^a, Hao Wei^{a}, Yiyong Mai^{a*}, and Xinliang Feng^b*

^a School of Chemistry and Chemical Engineering, School of Electronic Information and Electrical Engineering, Shanghai Key Laboratory of Electrical Insulation and Thermal Ageing, Shanghai Jiao Tong University, 800 Dongchuan RD, Shanghai 200240, P. R. China

^b Department of Chemistry and Food Chemistry, Technische Universität Dresden, Mommsenstrasse 4, 01062 Dresden, Germany

Email: mai@sjtu.edu.cn (Y. M.); haowei@sjtu.edu.cn (H. W.)

1. Experimental Section

1.1 *Materials*: Monomethoxy poly (ethylene oxide) (monomethoxy-PEO5000), CuBr, triethylamine, 2-bromoisobutyrylbromide, bipyridine, styrene, MoS₂ powders, P123 and toluene were purchased from Sigma-Aldrich. Methanol, ether, anhydrous ethanol, tetrahydrofuran (THF), aniline and ammonium persulfate (APS) were purchased from Sinopharm Chemical Reagent Co. Ltd. Other chemicals were purchased from Aladdin Reagent (Shanghai) and used without further purification.

1.2 *Synthesis of PS-*b*-PEO copolymers*: The PS-*b*-PEO diblock copolymers with different molecular weights (i.e. PS₆₀-*b*-PEO₁₁₄, PS₁₀₀-*b*-PEO₁₁₄, where the numbers denotes the degrees of polymerization of the corresponding blocks) were prepared by a living ATRP method including two steps. The first step involved the synthesis of macroinitiator PEO₁₁₄-Br according to the reported procedures.¹ In the second step, 2g PEO₁₁₄-Br macroinitiator (3.8×10^{-3} mol) was placed in a 200 mL two-neck schlenk flask equipped with a septum. Then, 0.034g CuBr (2.4×10^{-3} mol) along with 0.11g bipyridine (1.5×10^{-2} mol) were added and the flask was evacuated and refilled with N₂ in several cycles in order to remove the oxygen. In a separate schlenk tube, 4 mL (3.5×10^{-2} mol) freshly distilled styrene was deoxygenated by bubbling N₂ gas for at least 0.5 hour. The styrene was then transferred to the macroinitiator flask via a double-tipped needle; the resulting dark-brown mixture was stirred at room temperature for 10 minutes and further deoxygenated by three freeze-and-thaw cycles. The mixture was cooled to room temperature and then placed in a thermostated oil-bath with a temperature of 120 °C, followed by stirring for 8 hours. The polymerization was quenched by the addition of a large amount of THF solvent and exposure to air. The mixture was passed through a short column of basic alumina and then precipitated into a large excess of methanol. The precipitate was filtered and then washed with methanol. The final product was dried under vacuum at 40 °C for 2 days.

1.3 Characterizations

Nuclear Magnetic Resonance (NMR) spectra were recorded in deuterated solvents on a Mercury Plus 400 (400 MHz for proton) spectrometer at room temperature with tetramethylsilane as the internal reference. Gel permeation chromatography (GPC) analyses were carried out on a Shimadzu Prominence system with a refractive index detector

(Shimadzu RID-10A) at 40 °C, using THF as the eluent and polystyrene (PS) as the standard. Scanning electron microscopy (SEM) observations were performed on a FEI Sirion-200 (FEI Co., USA) field emission scanning electron microscope at 10 kV. Transmission electron microscopy (TEM) measurements were performed on a JEOL-2100 (JEOL Ltd., Japan) at an accelerating voltage of 200 kV. X-Ray photoelectron spectroscopy (XPS) was conducted on an AXIS Ultra DLD system (Kratos Co., Japan) with Al K α radiation as the X-ray source. All the binding energies were calibrated via referencing to C1s binding energy (284.6 eV). Nitrogen adsorption isotherms were measured at 77K on an Autosorb-iQA3200-4 sorption analyzer (Quantatech Co., USA) instrument. Before measurement, samples were degassed in a vacuum at 150 °C for at least six hours. Brunauer-Emmett-Teller (BET) method was utilized to calculate the specific surface area using adsorption data in a relative pressure range from 0.06 to 0.2. The pore size distributions were derived from the adsorption branches of isotherms using Barrett-Joyner-Halenda (BJH) method, and the total pore volumes were estimated from the adsorbed amount at a relative pressure P/P₀ of 0.99 specific surface areas. Raman measurement was conducted on an Invia/Reflrx Laser Micro-Raman spectrometer (Renishaw, England) excited by a laser beam of 532 nm. Powder XRD patterns were recorded on a Rigaku X-ray diffractometer D/MAX-2200/PC at a rate of 0.6 °min⁻¹ over the range 5-80° (2 θ). Fourier-transform infrared spectra between 4,000 and 400 cm⁻¹ were recorded using a Nicolet iS10. Atomic Force Microscopy (AFM) images were recorded in air on Dimension Icon & FastScan Bio. Inductively Coupled Plasma (ICP) spectrometry was performed on iCAP7600.

2. Figures and Tables

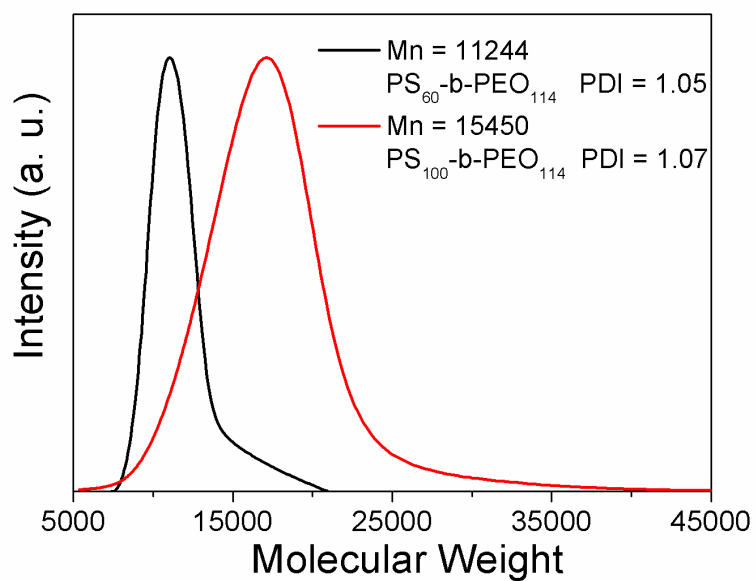


Figure S1. GPC curves of PS₆₀-b-PEO₁₁₄ and PS₁₀₀-b-PEO₁₁₄

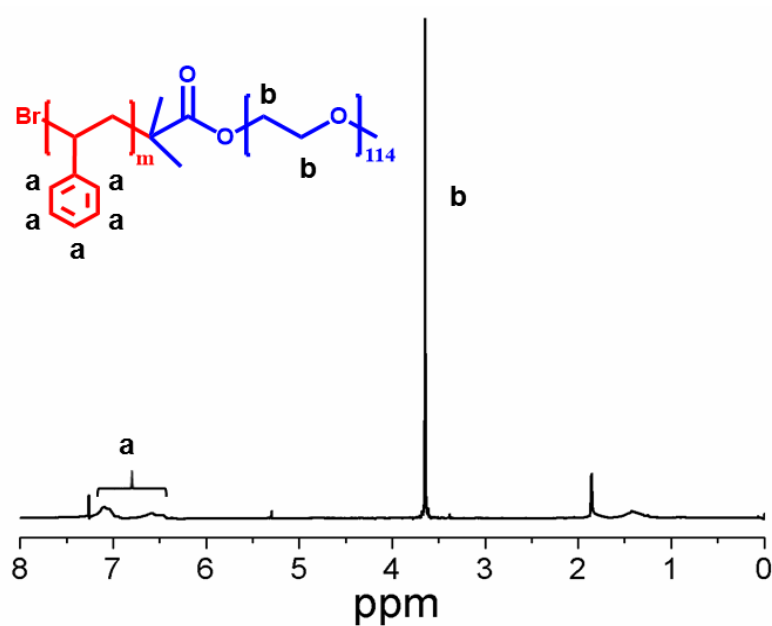


Figure S2. Typical ¹H NMR spectrum of PS_m-b-PEO₁₁₄

Herein, the ¹H NMR spectrum of PS₆₀-b-PEO₁₁₄ is shown as an example. From the spectrum, the degree of polymerization (*DP*) of PS can be calculated as follows:

$$DP_{ps} = \frac{I_a / 5}{I_b / 4} \times 114 \approx 62$$

In the equation, I_a is the integrated value of the proton peaks attributed to phenyl groups of PS block (signal **a**), I_b represents the integrated value of the proton peaks attributed to PEO block (signal **b**). 114 is the DP of the PEO block. Similarly, DP_{ps} of PS₁₀₀-*b*-PEO₁₁₄ calculated according to NMR spectrum is 102, which is very close to that calculated by GPC.

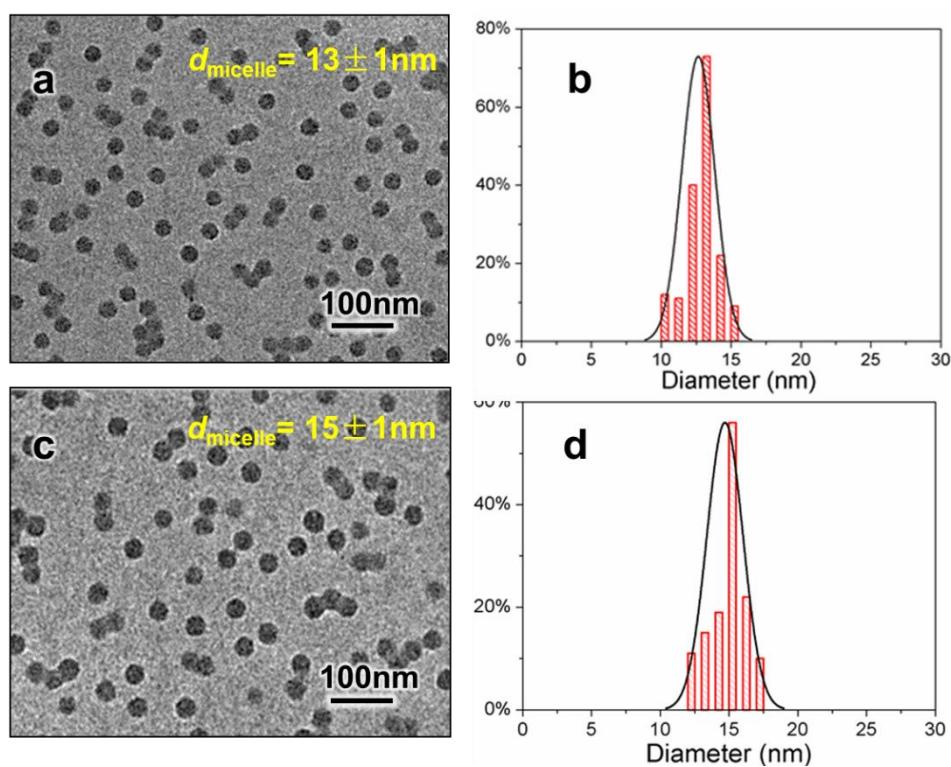


Figure S3. TEM images and size distribution histograms of PS-*b*-PEO micelles based on statistics of 500 particles. (a, b) PS₆₀-*b*-PEO₁₁₄, (c, d) PS₁₀₀-*b*-PEO₁₁₄.

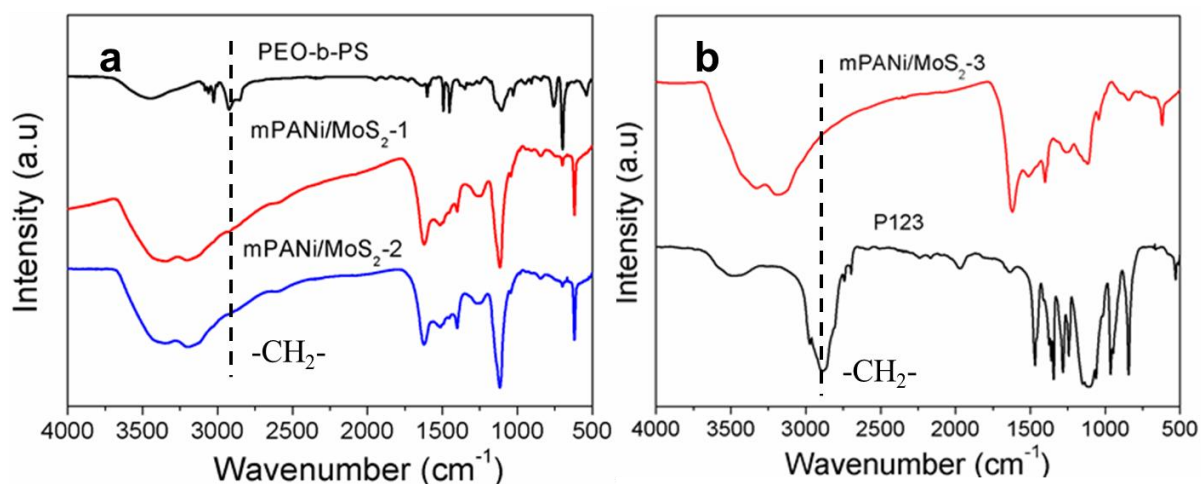


Figure S4. FTIR Spectra of (a) PS-*b*-PEO, mPANi/MoS₂-1 and mPANi/MoS₂-2; (b) P123 and mPANi/MoS₂-3. The disappearance of the signals attributed to PS-*b*-PEO or P123 in the spectra of mPANi/MoS₂-1&2 or mPANi/MoS₂-3 indicates the complete removal of the copolymer templates.

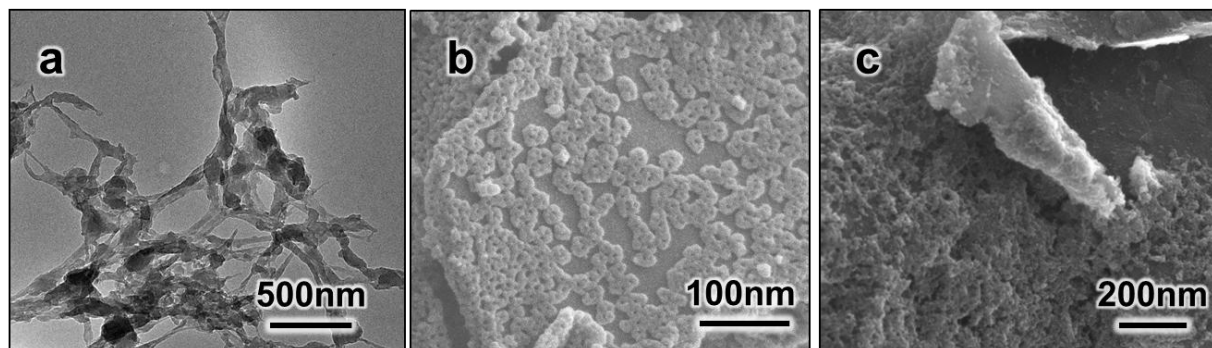


Figure S5. Electron Microscope images of pure PANi (a) and mPANi/MoS₂ (b, c) with different amounts of aniline. (b) PS-*b*-PEO 0.03 g, aniline 35 μ L; (c) PS-*b*-PEO 0.1 g, aniline 105 μ L.

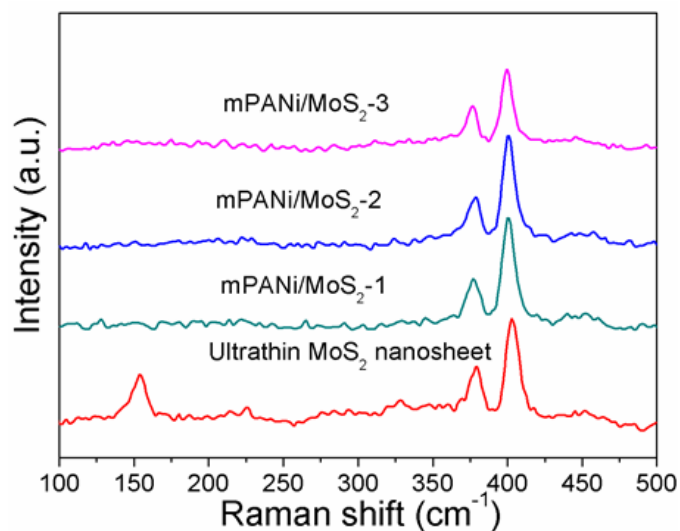


Figure S6. Raman spectra of ultrathin MoS₂ nanosheets, mPANi/MoS₂-1, mPANi/MoS₂-2 and mPANi/MoS₂-3. In the spectra of the mPANi/MoS₂ samples, the great attenuation of the signal at ca. 150 cm⁻¹, which originates from ultrathin MoS₂ sheets, is ascribed to the coating of the PANi layer according to literature.²

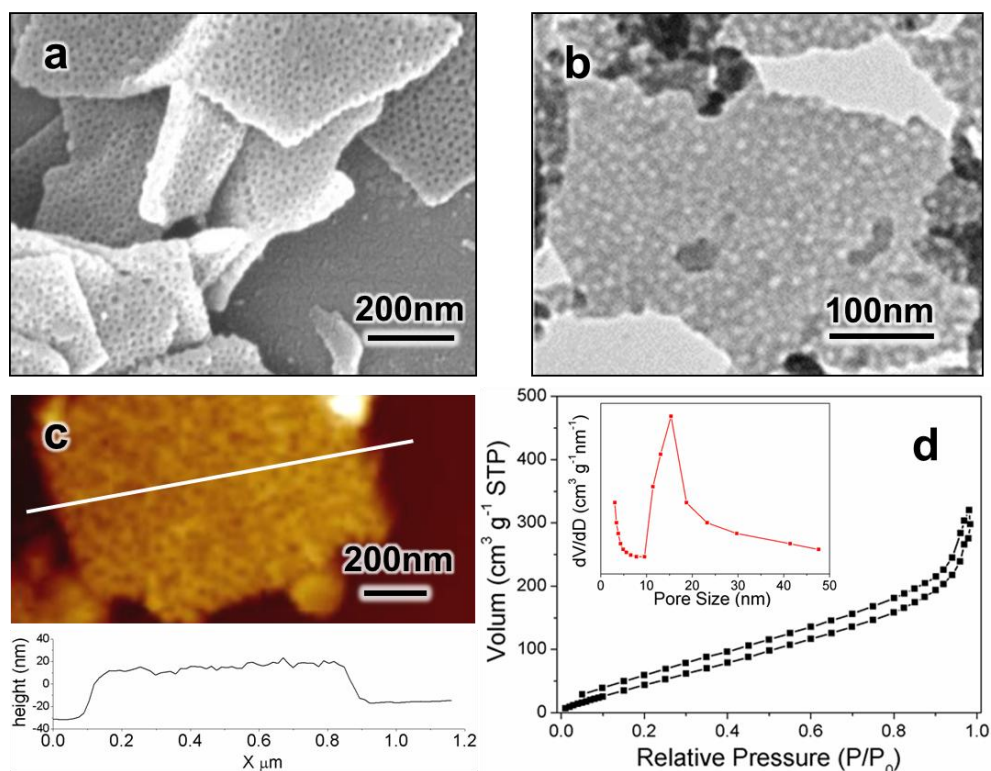


Figure S7. Structural characterizations of mPANi/MoS₂-2. (a) SEM image. (b) TEM image. (c) AFM height profile. (d) Nitrogen adsorption–desorption isotherms, the inset shows the corresponding pore size distribution.

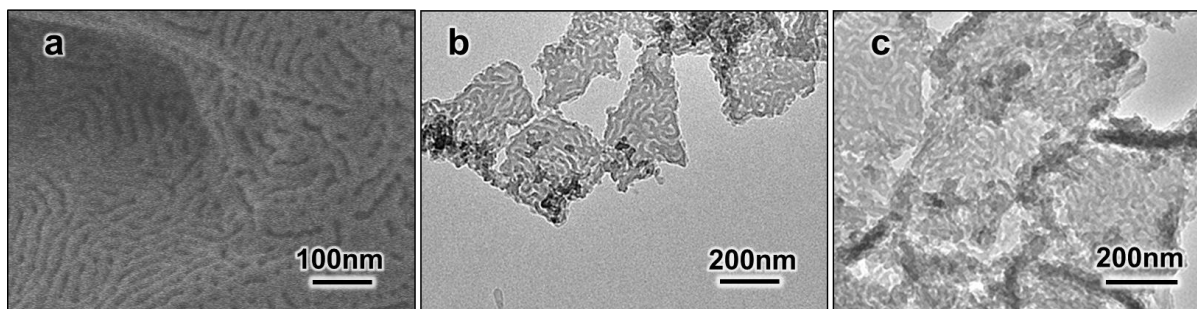


Figure S8. Representative Electron Microscope images of mPANi/MoS₂-3. (a) SEM; (b,c) TEM.

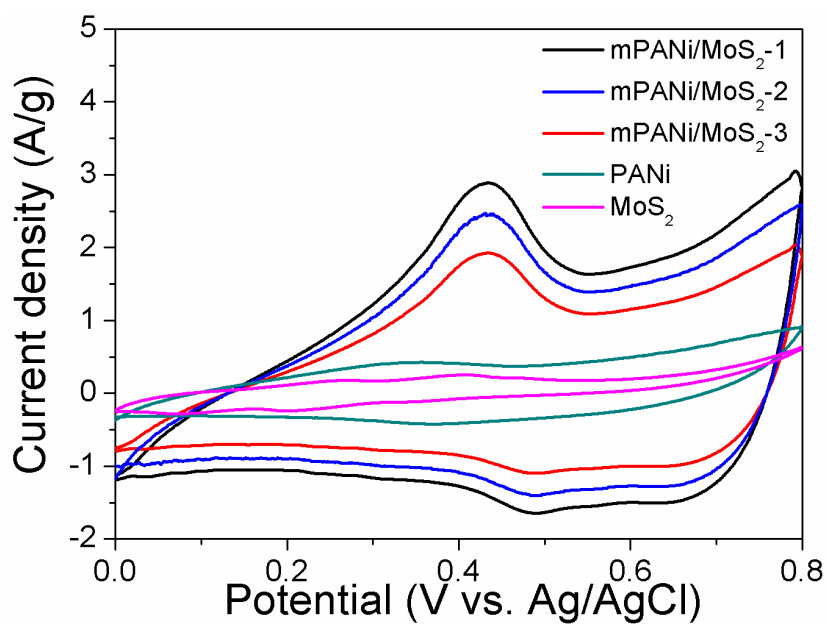


Figure S9. CV curves of mPANi/MoS₂-1, mPANi/MoS₂-2, mPANi/MoS₂-3, PANi and MoS₂ as electrodes recorded at scan rate of 10 mV s⁻¹ in 1 M H₂SO₄ electrolyte.

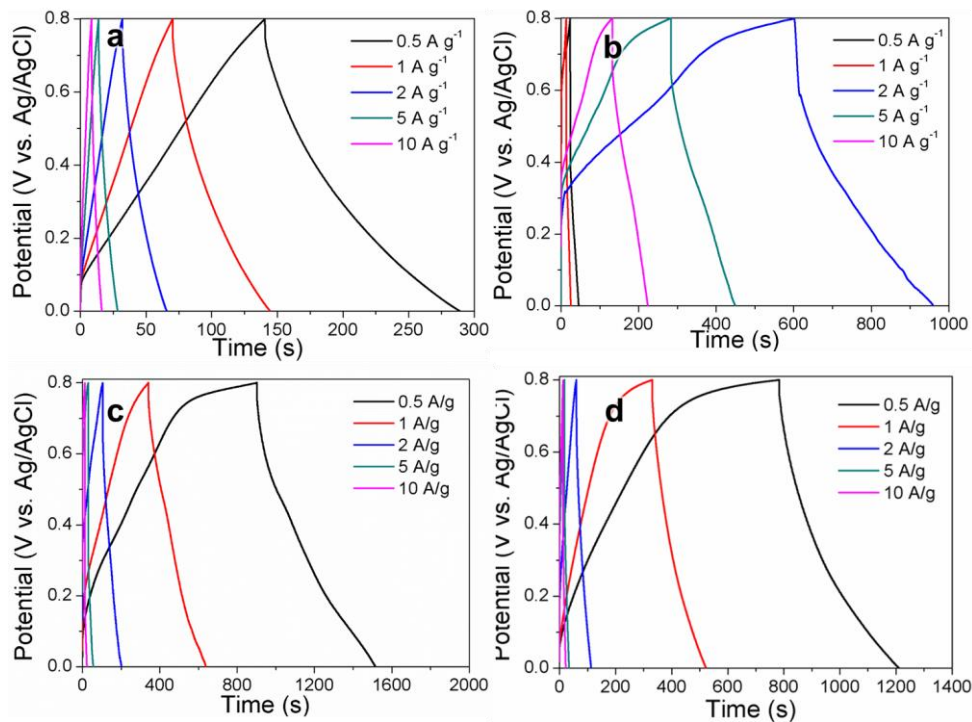


Figure S10. Galvanostatic charge/discharge curves for MoS₂ nanosheet (a), PANi (b), mPANi/MoS₂-2 (c) and mPANi/MoS₂-3 (d) at different current densities in 1 M H₂SO₄ electrolyte.

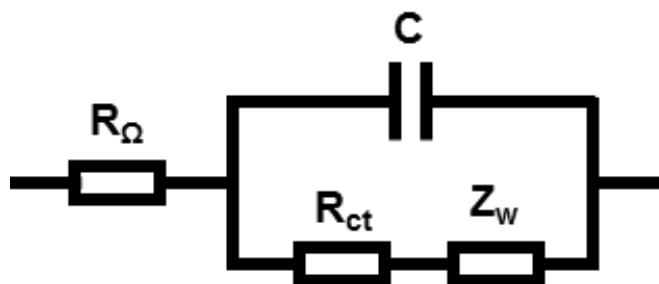


Figure S11. The equivalent circuit, in which R_{Ω} represents series resistance, C denotes constant phase element, R_{ct} stands for charge transfer resistance and Z_w is Warburg impedance.

Table S1. Comparison of electrochemical performance of mPANI/MoS₂-1 in our work and some related nanomaterials in reported literature

Materials	Specific capacitance (F/g)	Electrolyte	Literature
mPANI/MoS ₂ -1	500 (0.5A/g)	1 M H ₂ SO ₄	This work
Metallic 1T phase MoS ₂ nanosheets	110 (1A/g)	0.5 M K ₂ SO ₄	Ref. 3
microporous carbon/1T MoS ₂ nanosheet	344 (0.2A/g)	6 M KOH	Ref. 4
ZIF-8 based microporous carbon/2H MoS ₂ nanosheet	189 (1 A/g)	1 M H ₂ SO ₄	Ref. 5
Crosslinked PANI nanorods	162 (1A/g)	1 M H ₂ SO ₄	Ref. 6
PANI nanoarrays/MoS ₂	425 (1A/g)	0.5 M H ₂ SO ₄	Ref. 7
PANI/Few layered MoS ₂ nanosheets	417 (0.2 A/g)	2 M H ₂ SO ₄	Ref. 8
PANI/1T MoS ₂ nanosheet MoS ₂ @C	305 (1 A/g)	1 M H ₂ SO ₄	Ref. 9
2D MoS ₂ /RGO	235 (5 mV/ s)	1 M H ₂ SO ₄	Ref. 10
PANI/3D tubular MoS ₂	552 (0.5 A/g)	1 M H ₂ SO ₄	Ref. 11
PANI nanofibers film/RGO	210 (0.3 A/g)	1 M H ₂ SO ₄	Ref. 12
PANI/RGO hybride film	431 (0.45 A/g)	1 M H ₂ SO ₄	Ref. 13

References

1. Mai, Y.; Eisenberg, A., Controlled Incorporation of Particles into the Central Portion of Vesicle Walls. *J Am Chem Soc* **2010**, *132*, 10078-10084.
2. Tang, H.; Wang, J.; Yin, H.; Zhao, H.; Wang, D.; Tang, Z., Growth of Polypyrrole Ultrathin Films on MoS₂ Monolayers as High-Performance Supercapacitor Electrodes. *Adv. Mater.* **2015**, *27*, 1117-1123.
3. Acerce, M.; Voiry, D.; Chhowalla, M., Metallic 1T phase MoS₂ nanosheets as supercapacitor electrode materials. *Nat. Nano.* **2015**, *10*, 313-318.
4. Yuan, K.; Zhuang, X.; Fu, H.; Brunklaus, G.; Forster, M.; Chen, Y.; Feng, X.; Scherf, U., Two-Dimensional Core-Shelled Porous Hybrids as Highly Efficient Catalysts for the Oxygen Reduction Reaction. *Angew. Chem. Int. Ed.* **2016**, *55*, 6858-6863.
5. Weng, Q.; Wang, X.; Wang, X.; Zhang, C.; Jiang, X.; Bando, Y.; Golberg, D., Supercapacitive energy storage performance of molybdenum disulfide nanosheets wrapped with microporous carbons. *J Mater. Chem. A* **2015**, *3*, 3097-3102.
6. Wang, X.; Deng, J.; Duan, X.; Liu, D.; Guo, J.; Liu, P., Crosslinked polyaniline nanorods with improved electrochemical performance as electrode material for supercapacitors. *J Mater. Chem. A* **2014**, *2*, 12323-12329.
7. Zhu, J. X.; Sun, W. P.; Yang, D.; Zhang, Y.; Hoon, H. H.; Zhang, H.; Yan, Q. Y., Multifunctional Architectures Constructing of PANI Nanoneedle Arrays on MoS₂ Thin Nanosheets for High-Energy Supercapacitors. *Small* **2015**, *11*, 4123-4129.
8. Gopalakrishnan, K.; Sultan, S.; Govindaraj, A.; Rao, C. N. R., Supercapacitors based on composites of PANI with nanosheets of nitrogen-doped RGO, BC1.5N, MoS₂ and WS₂. *Nano Energy* **2015**, *12*, 52-58.
9. Yang, C.; Chen, Z.; Shakir, I.; Xu, Y.; Lu, H., Rational synthesis of carbon shell coated polyaniline/MoS₂ monolayer composites for high-performance supercapacitors. *Nano Res.* **2016**, *9*, 951-962.
10. Da Silveira Firmiano; Edney Geraldo; Rabelo, A. C.; Dalmaschio, C. J.; Pinheiro, A. N.; Pereira, E. C.; Schreiner, W. H.; Leite, E. R., Supercapacitor Electrodes Obtained by Directly Bonding 2D MoS₂ on Reduced Graphene Oxide. *Adv. Energy Mater.* **2014**, *4*, 1301380.

11. Ren, L. J.; Zhang, G. N.; Yan, Z.; Kang, L. P.; Xu, H.; Shi, F.; Lei, Z. B.; Liu, Z. H., Three-Dimensional Tubular MoS₂/PANI Hybrid Electrode for High Rate Performance Supercapacitor. *Acs Appl. Mater. Inter* **2015**, *7*, 28294-28302.
12. Wu, Q.; Xu, Y. X.; Yao, Z. Y.; Liu, A. R.; Shi, G. Q., Supercapacitors Based on Flexible Graphene/Polyaniline Nanofiber Composite Films. *Acs Nano* **2010**, *4*, 1963-1970.
13. Kim, M.; Lee, C.; Jang, J., Fabrication of Highly Flexible, Scalable, and High-Performance Supercapacitors Using Polyaniline/Reduced Graphene Oxide Film with Enhanced Electrical Conductivity and Crystallinity. *Adv. Funct. Mater.* **2014**, *24*, 2489-2499.